



Cite this: *Environ. Sci.: Nano*, 2025, 12, 5226

Host and microbiome proteins in eco-coronas: abundance, physicochemical properties and binding partners

Bregje W. Brinkmann, ^{*,a} Zhiling Guo, ^b Martina G. Vijver, ^a
Willie J. G. M. Peijnenburg ^{ac} and Andrew J. Chetwynd ^d

Nanoparticles sequester biomolecules from their immediate surroundings through chemi- and physisorption interactions. In ecosystems, these biomolecules form a transient ‘face’ on the particle surface, termed the eco-corona. Through bio-nano interactions, proteins of host-associated microbiomes can interact with eco-coronas, potentially altering the identity and behavior of nanomaterials. Here, microbiome proteins in eco-coronas from the common ecotoxicological tests species *Daphnia magna* and *Danio rerio* were characterized on carbon nanotubes and titanium dioxide nanoparticles using a combination of LC-MS/MS-based proteomics and metagenomic sequencing. In total, 520 *D. magna* proteins, 1444 *D. rerio* proteins, and 1405 and 441 proteins of their respective microbiomes were identified. Analysis of their binding partners indicated that these host and microbiome proteins can facilitate the additional recruitment of anions, cations, proteins, carbohydrates and lipids in eco-coronas. In terms of their physicochemical properties, microbiome proteins were smaller and provided areas with higher polarity and more cationic charge than host proteins. These results thereby reveal how microbiome proteins can alter nanomaterial surface properties. Furthermore, the present study suggests that the identity of microbiome proteins in eco-coronas can provide useful information on nanomaterial transport through ecosystems, especially when experimental studies on microbiome-nanomaterial interactions are executed in the presence of the host.

Received 18th May 2025,
Accepted 26th September 2025

DOI: 10.1039/d5en00493d

rsc.li/es-nano

Environmental significance

When nanomaterials enter ecosystems, multiple layers of biomolecules adsorb on their once bare surface. This so-called ‘eco-corona’ contributes to surface interactions that govern the recognition, diffusion and toxicity of nanomaterials in the environment. Little is known about the contribution of secreted proteins from host-associated microbiomes to eco-coronas. In this study, we show that secreted proteins from the microbiomes of *Daphnia magna* and *Danio rerio* become enriched in eco-coronas of carbon and metal nanomaterials. Importantly, these proteins contribute differently to the physicochemical properties and binding partners of eco-coronas than proteins originating from both hosts. Future applications of this knowledge include the use of host-specific microbiome proteins to decipher transport pathways of nanomaterials through ecosystems.

1. Introduction

When nanomaterials interact in ecosystems, flow through biofluids, and encounter cells, their fate is largely influenced by the physical, chemical, and biomolecular

features of the nano-surface. Nano-surface properties contribute to the identity of nanomaterials that is recognized by cells,¹ influence the transport of nanoparticles through extracellular matrices,² and affect their toxicity to biota.^{3–5} Recent bio-nanotechnological advancements allow the design and creation of nano-enabled products, including nano-pharmaceuticals and nano-agricultural, through precise engineering of nano-surface functionalities.⁶ Yet, once nanomaterials enter the body or any other environment, including ecosystems, they sequester biomolecules from their immediate surroundings, forming layers of adsorbed biomolecules.⁷ This alters the fate of the nanomaterials and the predictability of nano-bio interactions.

^a Institute of Environmental Sciences (CML), Leiden University, PO Box 9518, Leiden, 2300 RA, the Netherlands. E-mail: bregje.brinkmann@deltares.nl

^b School of Geography, Earth and Environmental Sciences, University of Birmingham, Birmingham, B15 2TT, UK

^c National Institute of Public Health and the Environment (RIVM), Center for Safety of Substances and Products, PO Box 1, Bilthoven, 3720 BA, the Netherlands

^d Centre for Proteome Research, Department of Biochemistry, Cell and Systems Biology, Institute of Systems, Molecular and Integrative Biology, University of Liverpool, L69 7BE, Liverpool, UK



Within the context of ecosystems, the biomolecular coat of nanomaterials is referred to as the eco-corona.^{8,9} Ecosystems comprise a great variety of biomolecules that can adsorb on the nano-surface,¹⁰ including proteins,¹¹ lipids,¹² bile salts,¹³ nucleic acids,¹⁴ extracellular polysaccharides,¹⁵ humic substances,¹⁶ and small (<1000 Da), polar, ionogenic metabolites like amino acids.¹⁷ The same process of adsorption based on abundance and affinity is assumed to form the basis for the interaction of this large variety of biomolecules with the nanosurface.¹⁰ Intermolecular interactions, such as the formation of protein–metabolite complexes, can additionally recruit metabolites into multilayered eco-coronas,¹⁰ where the order of bio–nano interactions was found to affect the final eco-corona composition.¹⁸ Small metabolites may furthermore bind by occupying the interstitial space in between larger proteins. These dynamic bio–nano interactions and large biomolecule availability make it extremely challenging to predict the spatiotemporal evolution of eco-coronas in the environment.¹⁹

To date, the composition and effects of eco-coronas have primarily been examined for natural organic matter^{17,18,20} and for biomolecules that originate from blood plasma, tissues, and mucosa from humans and other organisms.^{9–13} Fewer investigations consider the biomolecules that are produced and secreted by the microorganisms that colonize these ‘host’ tissues,^{21,22} collectively forming so-called host-associated microbiomes. Importantly, both host and microbiome biomolecules are not only present on and in biota but are also released into their direct surroundings, ‘conditioning’ these environmental matrices within minutes.²¹

In this study, we focus on the contribution of host-associated microbiomes to the protein eco-corona. We select this specific domain of the eco-corona because available technologies,²³ reference databases^{24–26} and bioinformatics tools^{27,28} allow us to infer the source, physicochemical properties, and potential binding partners of coronal proteins. This is essential to elucidating the role of host-associated microbiomes in eco-corona formation. Moreover, the identification of eco-corona proteins can reveal what adverse outcome pathways are associated with bio–nano interactions in the environment, thereby deepening our mechanistic understanding of nanomaterial toxicity.²⁹

The identification of microbiome proteins in eco-coronas can foster new nanotoxicological insight from two points of view. Firstly, it can aid in a more comprehensive identification of the actual composition of the protein eco-corona, comprising both host and microbiome proteins. This, in turn, can improve our understanding of surface properties that govern the recognition, transport and toxicity of nanomaterials. Secondly, proteins from host-associated microbiomes in eco-coronas could constitute a new source of information for the reconstruction of the transport pathways of nanomaterials through ecosystems. Because the composition of host-associated microbiomes does not solely

depend on host species³⁰ but also on its life stage, tissue type and health status,³¹ the identification of microbiome proteins in eco-coronas can eventually lead to more detailed identifications of the organisms and tissues that had been exposed to nanomaterials in the environment.⁹

To set the ground for these new research opportunities, we identified microbiome proteins in eco-coronas of titanium dioxide nanoparticles (nTiO₂) and multi-walled carbon nanotubes (CNTs) using liquid chromatography–mass spectrometry (LC–MS/MS). These eco-coronas were formed using proteins that were secreted by two common aquatic ecotoxicological test species into their culture media. These two test species included neonates of the water flea *Daphnia magna*, employed following OECD test guideline No. 202,³² and larvae of the zebrafish *Danio rerio*, employed following OECD test guideline No. 236.³³ In addition to their proven ecotoxicological value, these bioindicator species provide access to complete reference genomes^{29,34,35} and support the NC3Rs framework that is aimed to minimize animal suffering by replacing, reducing and refining traditional animal experimentation.^{29,36}

This eco-corona study consists of three parts. In the first part, we explore what proportion of eco-corona proteins can be retraced to the microbiomes of these test species. To this end, reference metagenomes were obtained from daphnids and zebrafish larvae. By comparing these reference metagenomes to the taxonomic assignment of reference proteomes, proteins of contaminating and free-living microbes were differentiated from proteins of host-associated microbes. In the next two parts of our study, we compare the composition of host and microbiome proteins in eco-coronas formed by *D. magna* and *D. rerio* under either germ-free or microbially colonized conditions. We first do so from a physicochemical perspective, deriving predictions of chemical and physical properties of eco-corona proteins using protein knowledge databases. We next take a functional perspective, predicting molecular binding partners of host and microbiome proteins in eco-coronas based on Gene Ontology (GO) molecular function annotations.

The results from this study highlight how microbiome proteins enrich eco-coronas in terms of their function and physicochemical properties. We identify five taxonomic groups of microbiome proteins that could serve as potential candidates for eco-corona-based reconstruction of nanomaterial transport pathways through ecosystems. Most of all, this study indicates that microbiome proteins in eco-coronas provide important interaction sites on nanomaterials, which can shape bio–nano interactions in a microbiome-dependent manner.

2. Methods

2.1 Pre-conditioning of culture media

2.1.1 *Daphnia magna* M7 medium. Daphnid neonates were obtained from a laboratory culture of 60 adult daphnids (*D. magna*; 2–3 weeks old) raised in Elendt M7 medium²⁴ at



22 °C with a relative humidity of 80%. Germ-free neonates were derived from 12 to 24 h old parthenogenetic eggs,³⁷ which were dissected from the brood pouch of adult daphnids, and sterilized following the protocol of Callens *et al.*³⁸ Briefly, eggs were incubated for 10 min in 0.01% peracetic acid in M7 and rinsed thrice with filter-sterilized M7 medium. Sterilized eggs were incubated for 2 d in filter-sterilized egg water. Microbially colonized neonates were collected from the culture within 24 h following their release from the brood pouch of adult daphnids. Given the life cycle of *D. magna*,³⁷ neonates are 3–4 d old at this stage.

Germ-free and microbially colonized daphnids were incubated for 48 h in filter-sterilized culture medium to collect their secreted proteins, at a density of 2 neonates per mL ($n = 3$). At the end of incubation, 3–5 neonates were collected for the quantification of colony-forming units (CFUs; File S1), and 45 neonates were sampled for metagenomic profiling (section 2.4). All selected neonates were rinsed thrice with filter-sterilized M7 to remove any loosely attached microbes. Neonates for metagenomic profiling were lysed in 180 μ L buffer ATL comprising 20 μ L proteinase K (DNeasy Blood & Tissue Kit; QIAGEN, Hilden, Germany). The remaining pre-conditioned M7 medium without neonates was used to form eco-coronas on the selected nanomaterials (section 2.2). Additionally, 1.5 mL of the pre-conditioned medium was freeze-dried for proteomic analysis (section 2.5).

2.1.2 Zebrafish larvae egg water. Zebrafish embryos were obtained from wild-type AB x TL zebrafish (*D. rerio*) housed at Leiden University's zebrafish facility in compliance with Dutch national regulation on animal experimentation ('Wet op dierproeven (Wod)' and 'Dierproevenbesluit 2014') and European animal welfare regulation (EU Animal Protection Directive 2010/63/EU). Standard protocols for zebrafish husbandry and experimentation (<https://zfin.org>) were followed in accordance with guidelines for the care and use of laboratory animals overseen by the Animal Welfare Body of Leiden University. All experiments were designed and conducted by an article 9 (Wod)-certified researcher using zebrafish larvae no older than 5 days post-fertilization (dpf). As larvae at this developmental stage do not feed independently, no license from the Centrale Commissie Dierproeven was required for these tests.

Embryos were collected in autoclaved egg water (60 mg L⁻¹ Instant Ocean artificial sea salt in demi water; Sera GmbH, Heinsberg, Germany). Half of the embryos were sterilized as described in detail in our previous study.³⁹ Briefly, the embryos were transferred to a mixture of ampicillin (100 μ g L⁻¹), kanamycin (5 μ g L⁻¹) and amphotericin B (250 ng L⁻¹) in autoclaved egg water for 6 h. Thereafter, the embryos were rinsed once for 45 s with a 0.2% PVP-iodine solution and were rinsed twice for 5 min with a 0.03% sodium hypochlorite solution (3.5% Cl₂). The other half of the embryos were not sterilized to raise microbially colonized larvae. Germ-free and colonized embryos were incubated in autoclaved egg water at 28 °C.

At 3 dpf, the zebrafish eggs had hatched, and their larvae were incubated for 48 h in a fresh solution of autoclaved egg water at 28 °C at a density of 5 larvae per mL ($n = 3$). This is in agreement with the test strategy developed by van Pomeroy *et al.*⁴⁰ At the end of incubation, 4 larvae were sampled for the quantification of CFUs (File S1), and 35 larvae were sampled for metagenomic profiling ($n = 3$; section 2.4). All selected larvae were rinsed thrice with autoclaved egg water to remove any loosely attached microbes. Larvae for metagenomic profiling were snap-frozen using liquid nitrogen in 800 μ L buffer AL of the DNeasy Blood & Tissue Kit (QIAGEN) and stored at -20 °C. The remaining egg water with secreted proteins was collected for the formation of eco-coronas (section 2.2). Additionally, 1.5 mL was sampled and freeze-dried for proteomic analysis (section 2.5).

2.2 Eco-corona formation

Eco-coronas were formed on titanium dioxide nanoparticles (nTiO₂) and carbon nanotubes (CNTs). We focus on nTiO₂ in the main text and provide methods and results for CNTs in the SI (File S2) for the reader that is specifically interested in this material.

Titanium dioxide nanoparticles of series NM-105 with a primary particle size of 15–24 nm were purchased from the European Commission's Joint Research Centre. The material consisted of a 12–19% rutile and 81–88% anatase crystalline phase, as determined by Rasmussen *et al.*⁴¹

Stock dispersions were prepared at a final concentration of 1.00 g L⁻¹ using a probe sonicator (Q125; Qsonica, Connecticut, USA) with a double stepped 1/8 inch microtip (4422; Qsonica, Connecticut, USA), following the dispersion protocol that was established in the NanoMILE project.⁴² Stocks for daphnid neonates were prepared in filter-sterilized M7 medium, and stocks for zebrafish larvae were prepared in autoclaved egg water. Two consecutive rounds of sonication were applied for 2 min in pulsed mode (1 s on : 1 s off) with a 30%-amplitude. This way, an acoustic power of 0.32 \pm 0.1 W was applied, as determined following the NANoREG sonicator calibration standard operation procedure (v 1.1).⁴³ Stock dispersions were shaken vigorously in between both sonication rounds.

Eco-coronas were formed by incubating nTiO₂ dispersions for 24 h at 22 °C at a final concentration of 100 mg L⁻¹ in the pre-conditioned medium of daphnid neonates and zebrafish larvae (section 2.1), under continuous agitation on an orbital shaker platform (200 rpm). This nTiO₂ concentration corresponds to the concentration of the limit test in the OECD test guidelines Nr. 202³² and Nr. 236.³³ At the end of incubation, particles were rinsed thrice in 100 mM ammonium bicarbonate (ABC) following the standard protocol of Zhang *et al.*²³ The pH of the ABC solution was set to 7.8 for daphnids and to 6.2 for zebrafish larvae to match the pH of M7 medium and egg water, respectively. Rinsed particles were freeze-dried and



stored at $-20\text{ }^{\circ}\text{C}$ until the samples were further prepared for proteomic profiling by LC-MS/MS (section 2.5).

2.3 Nanomaterial characterization

The size and shape of primary particles were characterized by way of transmission electron microscopy. To this end, particles from $5\text{ }\mu\text{L}$ of a 10 mg L^{-1} dilution in demi water were transferred to a copper-mesh grid. After at least 24 h of drying, grids were imaged using a JEOL 1400 microscope (Jeol Ltd., Tokyo, Japan).

The hydrodynamic size of aggregates was measured at 0 h and 2 h following dispersion in sterilized medium (at 10 mg L^{-1}) by way of dynamic light scattering using a Zetasizer Ultra instrument (Malvern Panalytical, Malvern, UK). The standard operation procedure delivered in NANoREG was followed (v 1.1),⁴⁴ with the adaptations reported in our previous study.³⁹

2.4 Metagenomic profiling of host-associated microbiomes

DNA was extracted from fresh daphnid lysate and frozen zebrafish larvae as described in the SI (File S1). Next-generation sequencing (NGS) of metagenomes was performed by BaseClear, Leiden, using the Illumina NovaSeq 6000 platform. For each of the samples, DNA libraries were prepared using the Nextera XT Library Preparation Kit. The libraries were sequenced at a sequencing depth of 2GB per sample. The *bc12fastq* conversion software (v. 2.20; Illumina, San Diego, CA, USA) was used to generate FASTQ read sequence files. Data passing Illumina Chastity filtering were cleaned up by removing any reads containing PhiX control signal and by clipping any reads containing (partial) adapters up to a minimum read length of 50 bp. The quality of the remaining reads was determined using the FASTQC quality control tool (Illumina; v. 0.11.8). *De novo* metagenome assembly was performed based on contigs ≥ 1000 bp using MEGAHIT (v. 1.2.9; <https://github.com/voutcn/megahit>).

2.5 Proteomic profiling of eco-coronas

2.5.1 Protein digestion. The methods for protein digest were as previously described^{23,45} with minor modification. In short, samples were resuspended in $20\text{ }\mu\text{L}$ of 10 mM dithiothreitol solution for reduction at $80\text{ }^{\circ}\text{C}$ for 10 min. This was followed by alkylation of the samples with the addition of $20\text{ }\mu\text{L}$ of 55 mM iodoacetamide which was left in the dark for 30 min at room temperature. The iodoacetamide was quenched with the addition of $9.4\text{ }\mu\text{L}$ of the dithiothreitol solution. Samples were digested for 16 h *via* the addition of a 1:1 ratio of trypsin and LysC at a 50:1 protease-to-protein ratio. The proteases were reconstituted in 0.1% Rapigest™ to aid in digestion and prevent reabsorption of digested peptides to the nanomaterials. Following digestion, the Rapigest™ was cleaved with the addition of $20\text{ }\mu\text{L}$ of 0.1 M hydrochloric acid. Peptides were subsequently enriched *via* zip tip enrichment and dried using a vacuum concentrator.

2.5.2 Liquid chromatography–mass spectrometry. Samples were reconstituted in $50\text{ }\mu\text{L}$ 0.1% formic acid and diluted to $5\text{ ng }\mu\text{L}^{-1}$ according to NanoDrop determination of protein concentration. Samples were loaded onto Evotips and injected on an EvoSep One LC system (Billedskaerervej, Denmark) running a 30 sample per day program with mobile phase A as 0.1% formic acid in water and mobile phase B being 0.1% formic acid in acetonitrile. Samples were separated on a $2\text{ }\mu\text{m} \times 100\text{ }\text{Å} \times 150\text{ }\mu\text{m} \times 15\text{ cm}$ PepMap RSLC C18 column (ThermoScientific, Bremen, Germany) and eluted onto a ThermoScientific (San Jose, CA, USA) Orbitrap Exploris 480 mass spectrometer equipped with a FAIMS Pro™ device which obtained data in a data-independent acquisition protocol. The MS was operated in positive ionization mode with a capillary voltage of 2200 V. MS1 was collected at FAIMS compensation voltages (CVs) of -40 and -60 V at a resolution of 120 000 between 345 and 900 *m/z* with a normalized AGC target of 300%. MS2 was collected in both FAIMS CVs at a resolution of 15 000 with a normalized collision energy of 32; the mass range was evenly split into 42 *m/z* windows with no overlap of 13 *m/z* between 350 and 896 *m/z* with a normalized AGC of 1000%.

2.6 Data analysis

2.6.1 Metagenomic classifications. Metagenomic data were classified and quantified following the step-by-step protocol for the Kraken suite published by Lu *et al.*⁴⁶ We performed the ‘microbiome analysis’ workflow in a Dev Container running the ‘jammy’ image of Ubuntu on an aarch63 architecture. All subsequent steps were performed using 12 threads.

First, host sequences were removed from NGS reads using Bowtie2 (v. 2.5.4).⁴⁷ For this purpose, genomic index files were generated for the host genome of *D. magna* ‘daphnmag2.4’ (GCA_001632505.1), obtained from the GenBank database (<https://www.ncbi.nlm.nih.gov/datasets/genome>) on 31 May 2024. Genomic index files for the *D. rerio* genome ‘GRCz11’ (GCF_000002035.6) were obtained from <https://benlangmead.github.io/aws-indexes/bowtie> on 28 May 2024.

Next, reads that did not align with the genome indices were classified using Kraken 2 (v. 2.1.3)⁴⁸ using the memory mapping option, setting the minimum number of hit-groups to 3. The PlusPF Kraken database (83 GB-index size), built on 5 June 2024 (<https://benlangmead.github.io/aws-indexes/k2>), was used as a reference for this taxonomic assignment. This 86 GB database includes the NCBI’s RefSeq public repository⁴⁹ for archaea, bacteria, viruses, plasmids, humans, UniVec_Core, protozoa and fungi.

Finally, Bracken (v. 2.9)⁵⁰ was used to quantify the relative abundance of identified microbial species based on a read length of 100 bp. Species with fewer than 10 assigned reads were omitted. The interactive Pavian webtool (<https://fbreitwieser.shinyapps.io/pavian/>; accessed 25 October 2024)⁵¹ was used to generate a tabular overview of the



number of these reads per sample at each taxonomic rank of interest (*i.e.* phylum, clade, and genus).

2.6.2 Proteomic data analysis. Data from LC–MS analysis (section 2.5.2) were imported into Spectronaut v.14 (Biognosys AG, Schlieren, Switzerland). The digest enzyme was set to trypsin and LysC with up to 2 missed cleaves allowed with fixed modifications of carbamidomethylation of cysteine and variable oxidation of methionine. Precursor ion error tolerance was set at 10 ppm, and fragment ion error tolerance at 0.01 Da. The false discovery rate (FDR) was set at 1% (0.01) at the level of the peptide spectral match. Reference proteomes of the hosts (*D. magna* and *D. rerio*), all bacteria and all fungi were obtained from UniProt.

Data for identified proteins were processed in five steps. The first step focused on proteins with multiple identifications (*i.e.* multiple matching proteins from the reference protein database). For these proteins, one of the identified proteins was randomly drawn for downstream analysis. If these identified proteins included proteins belonging to microbial genera that were detected in corresponding metagenomes (section 2.6.1), one of these proteins was randomly selected. In the second step, the lysyl endopeptidase protein of *Pseudomonas aeruginosa* (accession Q02SZ7) was removed, since this enzyme was used to digest proteins for LC–MS analysis. In the third step, MS-intensities were \log_2 -transformed and median centered.⁵² In the fourth step, missing data of proteins that were only detected in 2 out of the 3 replicates were imputed by way of probabilistic minimum imputation.⁵³ Missing data for proteins that were detected in eco-coronas but were not identified in the medium were also imputed. Our approach was based on the assumption that missing data follow a narrowed downshifted normal distribution. The standard deviation for imputed data (σ_{imputed}) was defined based on the standard deviation of detected proteins (σ_{detected}) following: $\sigma_{\text{imputed}} = 0.3 \times \sigma_{\text{detected}}$. The mean of the imputed data (μ_{imputed}) was based on the mean of measured data (μ_{detected}) and σ_{detected} following: $\mu_{\text{imputed}} = \mu_{\text{detected}} - 1.8 \times \sigma_{\text{detected}}$. In the fifth step, microbial proteins that likely represented misidentifications were removed based on the assumption that microbial protein could only be detected in germ-free treatments if these proteins had been attached to the particles prior to eco-corona formation. Therefore, microbial proteins were removed if these were identified (1) in the germ-free coronas but neither in the germ-free medium nor in the blanks, (2) in both the blank and the medium, or (3) in the germ-free medium but not in any of the germ-free coronas. Proteins belonging to microbial genera represented by less than 5 proteins in the entire dataset were also removed to decrease the number of false detections.

2.6.3 Predictions of protein properties. Identified proteins were described in terms of their physicochemical properties and binding partners. Predictions of these properties were obtained from protein databases as described below.

The molecular weight (MW) and isoelectric point (pI) of proteins were obtained from the UniProtKB/Swiss-Prot

Protein knowledgebase²⁶ using the ‘Compute pI/Mw’ Expasy webtool (https://web.expasy.org/compute_pi; accessed 18 November 2024).^{54–56} Predictions for different isotopes were averaged. For 9 of the 2690 *D. magna* proteins and 11 of the 3294 *D. rerio* proteins, 2 predictions were obtained for the same UniProt accession number, which were averaged.

The AlphaFold Protein Structure database (v. 4)^{24,25} was used to obtain predictions of the solvent-accessible surface area (SASA) of proteins. The database was accessed on 18 November 2024 from a Linux Dev Container running the 1-3.12-bullseye Python 3 image. First, UniProt accession numbers of identified proteins were matched to AlphaFold IDs. Next, these AlphaFold IDs were used to retrieve PDB files from the AlphaFold database. Finally, the FreeSASA Python module (v. 2.2.1; <https://freesasa.github.io/python/intro.html>)²⁷ was used to compute the polar, apolar and total SASA of proteins based on the obtained PDB files. All proteins without MW, pI and/or total SASA predictions were excluded (2502 of 38 772 *D. magna* proteins and 7434 of 51 804 *D. rerio* proteins).

The binding partners of proteins were inferred based on molecular function Gene Ontology (GO) annotations. These annotations were obtained from the UniProtKB Protein knowledgebase on 18 November 2024 (<https://www.uniprot.org/id-mapping/>). The ‘ontologyIndex’ package (v. 2.12)²⁸ for R was used to download the ‘go-basic.obo’ ontology (<https://geneontology.org/docs/download-ontology/>; accessed 18 December 2024). Any descendant of GO:0005488 (‘binding’) was identified as a protein with a binding partner. More specifically, we differentiated the following five partners: (1) ‘cation binding’: any descendant of GO:0043169; (2) ‘anion binding’: any descendant of GO:0043168; (3) ‘carbohydrate binding’: any descendant of GO:0030246 or GO:0005529; (4) ‘lipid binding’: any descendant of GO:0008289; and (5) ‘protein binding’: any descendant of GO:0005515, GO:0001948 or GO:0045308.

2.6.4 Statistical tests. Metagenomic and proteomic data were analyzed and visualized using R (v. 4.4.1; <https://www.R-project.org/>), applying functions of the packages ‘readr’ (v. 2.1.5), ‘dplyr’ (v. 1.1.4), ‘car’ (v. 3.1-3), ‘tidyr’ (v. 1.3.1), ‘ggplot2’ (v. 3.5.1), ‘ggVennDiagram’ (v. 1.5.2), ‘taxonomizr’ (v. 0.10.6), ‘ape’ (v. 5.8) and ‘RColorBrewer’ (v. ‘1.1.3’). Means and standard errors of the mean (SEM) are presented, unless indicated otherwise.

The percentage of microbiome proteins in eco-coronas and in the surrounding medium was compared for daphnids and zebrafish using a two-way analysis of variance (ANOVA) test. The sample type (medium/eco-corona) and host species (daphnid/zebrafish) were included as the explanatory variables in this test. Total MS intensities of proteins originating from the host or microbiome were compared between the medium and the eco-coronas for daphnids and zebrafish separately by way of one-way ANOVA tests. Total MS intensities of germ-free proteins were also analyzed in a one-way ANOVA test.



Intensity-weighted average intensities of three of the four physicochemical protein properties (MW, total SASA and apolar:polar SASA) and the relative intensities of proteins with each of the binding partners were compared between both hosts (daphnids and zebrafish larvae), between the three protein origins (microbially colonized hosts, microbiomes, germ-free hosts), and between the medium and nTiO₂ eco-corona in a multi-way ANOVA test. Protein pI was compared in a similar design, but for cationic proteins (pI > pH) and anionic proteins (pI < pH) separately, due to the dependence of protein charge on pI, which violates the ANOVA assumptions. The relative fraction of cationic proteins in eco-coronas was compared for daphnids and zebrafish separately, comparing the three protein origins, for the medium and nTiO₂ eco-corona in a two-way ANOVA test.

Interactions between explanatory variables were included only in case these were significant, unless indicated differently in Table S1. The tests were combined with Tukey's HSD *post hoc* test. The Shapiro–Wilk test was performed to verify that the model's residuals were normally distributed. To meet this assumption, total MS intensities were log-transformed. For anions and lipids, log-transformation was also required for this purpose. In certain cases, proteins from daphnids and zebrafish were analyzed separately to ensure that the model's residuals followed a normal distribution (Table S1). The Levene's test from the R package 'car' was performed to check if the variance was equally spread across treatment groups.

3. Results and discussion

3.1 Nanomaterial characterization

The basis of this study is the comparison of eco-coronas formed by *D. magna* and *D. rerio* on nTiO₂. For the interested reader, similar results for CNTs are presented in the SI (File S2). Primary particles of nTiO₂ had irregular, angular shapes (Fig. 1), a width of 21.3 ± 1.2 nm and a length of 28.0 ± 1.5 nm ($n = 30$), as determined previously.⁵⁷ Additional measurements of the specific surface area, crystal phase, (surface) chemistry and hydrochemical reactivity have been reported by Rasmussen *et al.*⁴¹

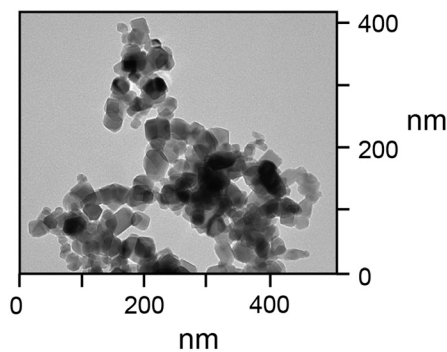


Fig. 1 Transmission electron microscopy photograph of TiO₂ nanoparticles.

Following dispersion in the culture medium, nTiO₂ nanoparticles formed micron-sized aggregates (Table S2). The mean hydrodynamic size of these aggregates was larger in the culture medium of *D. magna* (~5 to 6 μm) than in the culture medium of *D. rerio* (~3 to 4 μm). In view of the low stability of nTiO₂, these results should be treated with caution. However, given the clear difference in hydrodynamic sizes, these measurements nevertheless indicate that nTiO₂ particles were less stable in the culture medium of *D. magna* than in the culture medium of *D. rerio*. This may be caused by the higher salt concentration in the culture medium of *D. magna* (>500 mg total salt per L) than in that of *D. rerio* (60 mg total salt per L).

3.2 Abundance of host and microbiome proteins in eco-coronas

Eco-coronas were obtained by incubating nTiO₂ in medium comprising the secreted proteins of either germ-free or microbially colonized *D. magna* neonates and *D. rerio* larvae. LC-MS/MS analysis indicated that these pre-conditioned media comprised at least 2293 different proteins for *D. magna* and 2877 different proteins for *D. rerio*. Following corona formation, 2025 *D. magna* proteins and 2503 *D. rerio* proteins were identified on TiO₂ nanoparticles (Table 1). We note that replicate A of *D. rerio* medium is an outlier, considering the low number of proteins that was identified for this sample.

The majority of the identified proteins, that is, 1511 *D. magna* proteins and 1077 *D. rerio* proteins, had a microbial origin. Such microbial proteins could originate either from free-living microbes or from the microbiomes of *D. magna* and *D. rerio*. These microbiomes comprised $7.5 \pm 1.6 \times 10^3$ and $1.9 \pm 0.5 \times 10^3$ colony-forming units (CFUs) per individual of *D. magna* and *D. rerio*, respectively. No CFUs could be isolated for germ-free hosts, confirming the successful eradication of microbiomes for these hosts.

Table 1 Number of proteins detected in pre-conditioned test medium and eco-coronas formed by microbially colonized and germ-free *D. magna* and *D. rerio*

Host	Sample	Replicate	Microbially colonized conditions		Germ-free conditions		
			Total	Host	Microbiome	Total	Host
<i>D. magna</i>	Medium	A	965	288	672	564	556
		B	1085	319	760	366	361
		C	1012	290	717	570	561
	nTiO ₂	A	1456	181	1257	520	492
		B	1597	180	1395	495	475
		C	1625	198	1405	297	269
<i>D. rerio</i>	Medium	A	415	253	83	926	904
		B	1423	964	203	1667	1628
		C	1407	965	189	1660	1624
	nTiO ₂	A	1255	293	441	1444	1404
		B	1560	643	409	1029	994
		C	1552	650	400	1431	1384



In order to identify microbiome proteins, the composition of host-associated microbiomes of daphnid neonates and zebrafish larvae were profiled by way of shotgun metagenomic sequencing. In total, 28–32 million reads were obtained for *D. magna* and 14–31 million reads for *D. rerio* (Table S3). Most of these reads aligned to the genomes of *D. magna* (71–74%) and *D. rerio* (68–84%). About 7–12% of the remaining reads could be mapped to genomic sequences of archaea, bacteria, viruses, protozoa and fungi. According to UniProt taxonomic identifiers,²⁶ the source of 1486 *D. magna* proteins and 514 *D. rerio* proteins were microbes of genera that were also identified in these microbial reads. Our further analyses are based on the assumption that these proteins, from hereon named ‘microbiome proteins’, originate from the host-associated microbiomes of *D. magna* and *D. rerio*.

Notably, the proportion of microbiome proteins was significantly lower in media of *D. magna* ($70.2 \pm 0.4\%$) and *D. rerio* ($15.9 \pm 2.1\%$) than in eco-coronas of *D. magna* ($86.7 \pm 0.3\%$) and *D. rerio* ($29.0 \pm 3.1\%$) ($F_{1,9} = 925.4$, $p < 0.001$) (Table 1). Likewise, while the mean total MS intensity of microbiome proteins exceeded that of host proteins in both media and nTiO₂ eco-coronas ($F_{1,8} = 306.2$, $p < 0.001$), this difference was larger for nTiO₂ eco-coronas (Fig. 2A; $F_{1,8} = 91.0$, $p < 0.001$). These results suggest that microbiome proteins have higher binding affinities for nTiO₂ than host proteins. In contrast to *D. magna* eco-coronas, higher intensities of host proteins were detected in both the medium and the eco-coronas of *D. rerio* (Fig. 2B; $F_{1,9} = 8.13$, $p = 0.02$). This may result from the presence of yolk proteins and parentally derived proteins in samples from zebrafish larvae,⁵⁸ accounting for up to $35.3 \pm 1.9\%$ and the total MS-intensity in pre-conditioned medium, and $30.3 \pm 9.3\%$ of the MS-intensity in nTiO₂ eco-coronas (Table S4). Irrespectively, it

reveals that the proportion of microbiome proteins in eco-coronas is host species dependent. This indicates that host and microbiome proteins jointly shape bio-nano interactions. We further investigate this in section 3.4.

3.3 Taxonomic composition of eco-coronas

In total, 51 microbial genera could be identified at a relative read count $>0.2\%$ of the sample total in metagenomes obtained for *D. magna*, and 61 microbial genera could be identified at the same threshold in metagenomes of *D. rerio* (Fig. S2). This threshold of 0.2% was chosen as the highest threshold that allowed identification of fungi in metagenomic data and moreover allowed detection of as many genera as possible of the set that was previously isolated from our cultures. These are *Acinetobacter*, *Sphingomonas*, *Aeromonas*, *Microbacterium* and *Rhodococcus* for *D. magna*,⁵⁹ and *Bosea*, *Rhizobium*, *Sphingomonas*, *Phyllobacterium*, *Aeromonas*, *Delftia*, *Pseudomonas*, *Stenotrophomonas*, *Chryseobacterium*, *Microbacterium* and *Staphylococcus* for *D. rerio*.^{39,57} In eco-coronas, we detected proteins of 18 different genera for *D. magna* and proteins of 17 different genera for *D. rerio*. A comparison of the relative abundance of the reads and proteins that have been detected for these genera is presented in Fig. 3.

Most microbiome proteins in eco-coronas originated from bacteria, such as gammaproteobacteria of the genera *Stutzerimonas*, *Pseudomonas*, *Salmonella* and *Escherichia* as well as the betaproteobacteria *Delftia*. Bacteria of these clades were also detected at high relative abundances in the metagenomes of *D. magna* and *D. rerio*. This is in agreement with previous metagenomic profiling efforts for *D. magna* and *D. rerio*.^{60–62} Compared to bacterial proteins, much fewer fungal proteins were detected, with detections for only two genera (*Neurospora* and *Candida*) in exclusively the eco-coronas of *D. rerio*. No protozoan, archaeal or viral proteins could be detected, while protozoa and viruses were detected in metagenomes (Fig. S3). This higher representation of fungi, protozoa and viruses in metagenomic data, as compared to the proteomic data, may be attributed to the higher amount of data obtained from metagenomic sequencing (Table S4) than from proteomic analysis (Table 1).

The overall taxonomic composition of eco-coronas highly resembled that of proteins from media (Fig. 3A). The similarity between proteomic and metagenomic samples was much lower, which, amongst others, may result from differences in the reference databases that were used for the taxonomic identification of DNA and protein sequences. While this may hamper the use of taxonomic profiles of eco-coronas for the reconstruction of nanomaterial transport, the presence or absence of proteins from specific taxa may still prove useful for this purpose. For instance, proteins of the bacteria *Stutzerimonas* and *Diaphorobacter* were detected at relatively high intensities in eco-coronas of *D. magna*, while no proteins at all were detected for these genera in eco-

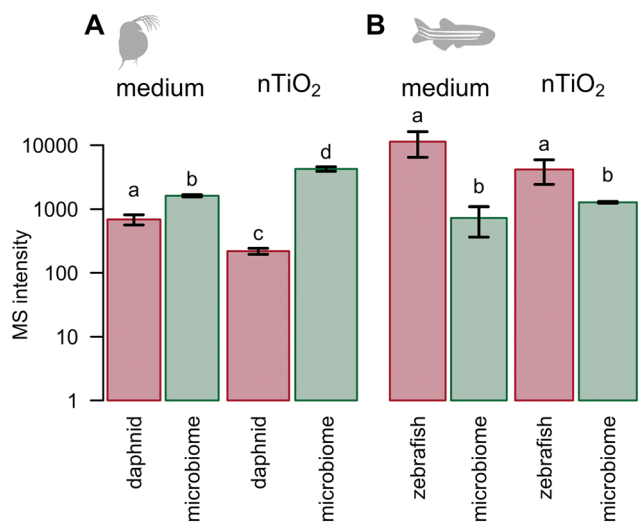


Fig. 2 Total intensity of proteins from hosts (red bars) and their microbiomes (green bars) in the medium and in nTiO₂ eco-coronas from *D. magna* (A) and *D. rerio* (B). Bars depict the means with SEM ($n = 3$). Bars that do not share a letter are significantly different ($p < 0.05$).



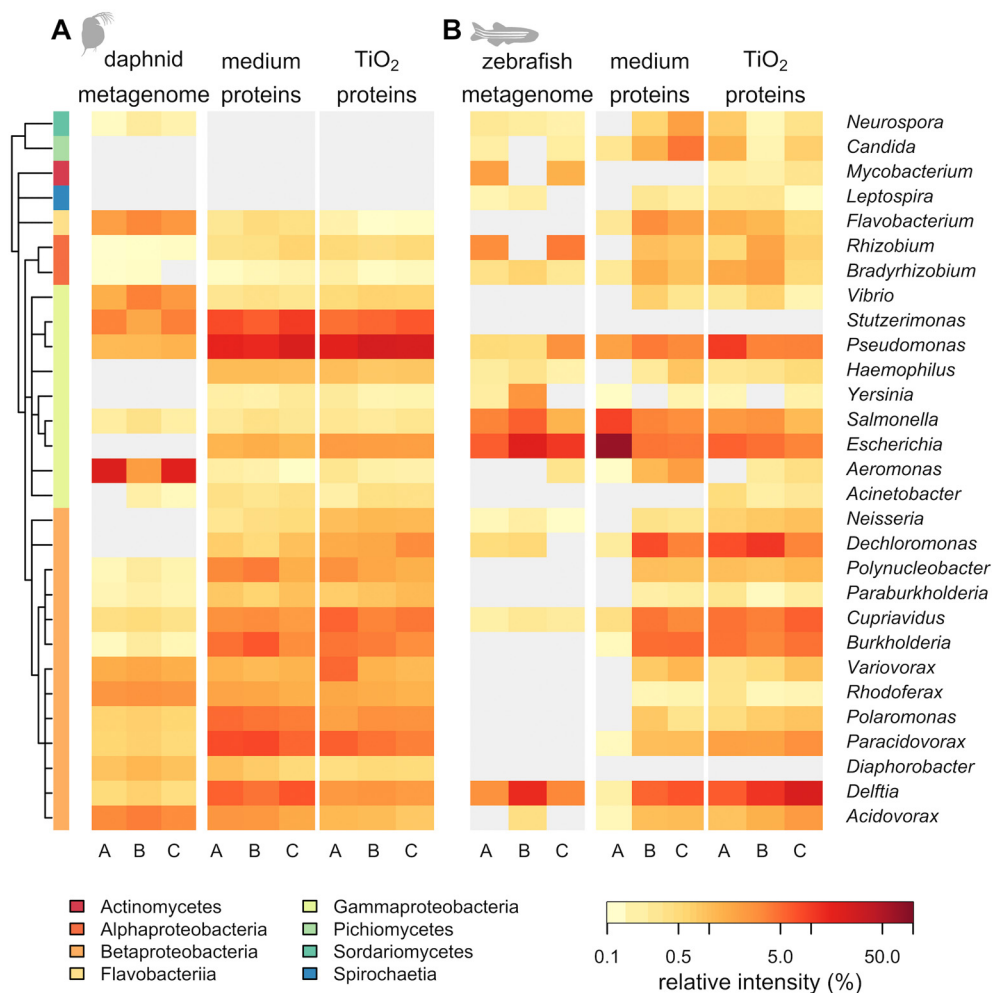


Fig. 3 Taxonomic composition of metagenomes and microbiome proteins in medium and nTiO₂ eco-coronas of daphnid neonates (A) and zebrafish larvae (B). Relative read abundance (% of sample total) and relative MS intensities (% of sample total) are shown for microbial genera with relative intensities >0.2%. The cladogram depicts ancestral relationships between microbial genera, where colors at cladogram tips correspond to microbial clades. Letters A–C (columns) refer to biological replicates. The light-grey shaded area indicates genera that have not been detected in the corresponding samples.

coronas of *D. rerio*. Similarly, fungal proteins of *Neurospora* and *Candida* were exclusively detected in eco-coronas of *D. rerio*. Hence, the presence of proteins from these taxa in eco-coronas could potentially inform what host species had been exposed to the concerning nanomaterials. This is particularly relevant considering the higher abundance of microbiome proteins than host proteins in eco-coronas, as discussed in the previous section (section 3.2).

Remarkably, the common symbiotic bacteria *Limnohabitans*, which colonizes the filter combs of *D. magna*,⁶³ could be detected only in *D. magna* metagenomes (Fig. S3). While the UniProt reference proteomes included 8 (pan-)proteomes of *Limnohabitans* (listed in Table S5), *Limnohabitans* proteins could not be detected using proteomics. This could indicate that the exchange of biomolecules between *Limnohabitans* bacteria and *D. magna* is confined to the filtering system of *D. magna*. It merits further investigation to find out if biomolecular traces of *Limnohabitans* and other symbionts alike only become part of

eco-coronas when nanomaterials are ingested. In view of the analytical challenges that are faced with the detection of internalized nanomaterials, which become part of complex biological matrices,⁶⁴ such markers could function as early indications for the ingestion of nanomaterials. When this source of eco-corona information is combined with quantitative approaches that can further reveal what fractions of ingested nanomaterials accumulate within animal tissue, this could significantly advance our understanding of the fate of ingested nanomaterials that possibly transfer within food chains.

3.4 Physicochemical properties of host and microbiome eco-corona proteins

In this section we compare four physicochemical properties of eco-corona proteins. These are (1) the molecular weight (MW) and (2) solvent-accessible surface area (SASA), as indications of protein size, (3) the polar-to-apolar SASA ratio



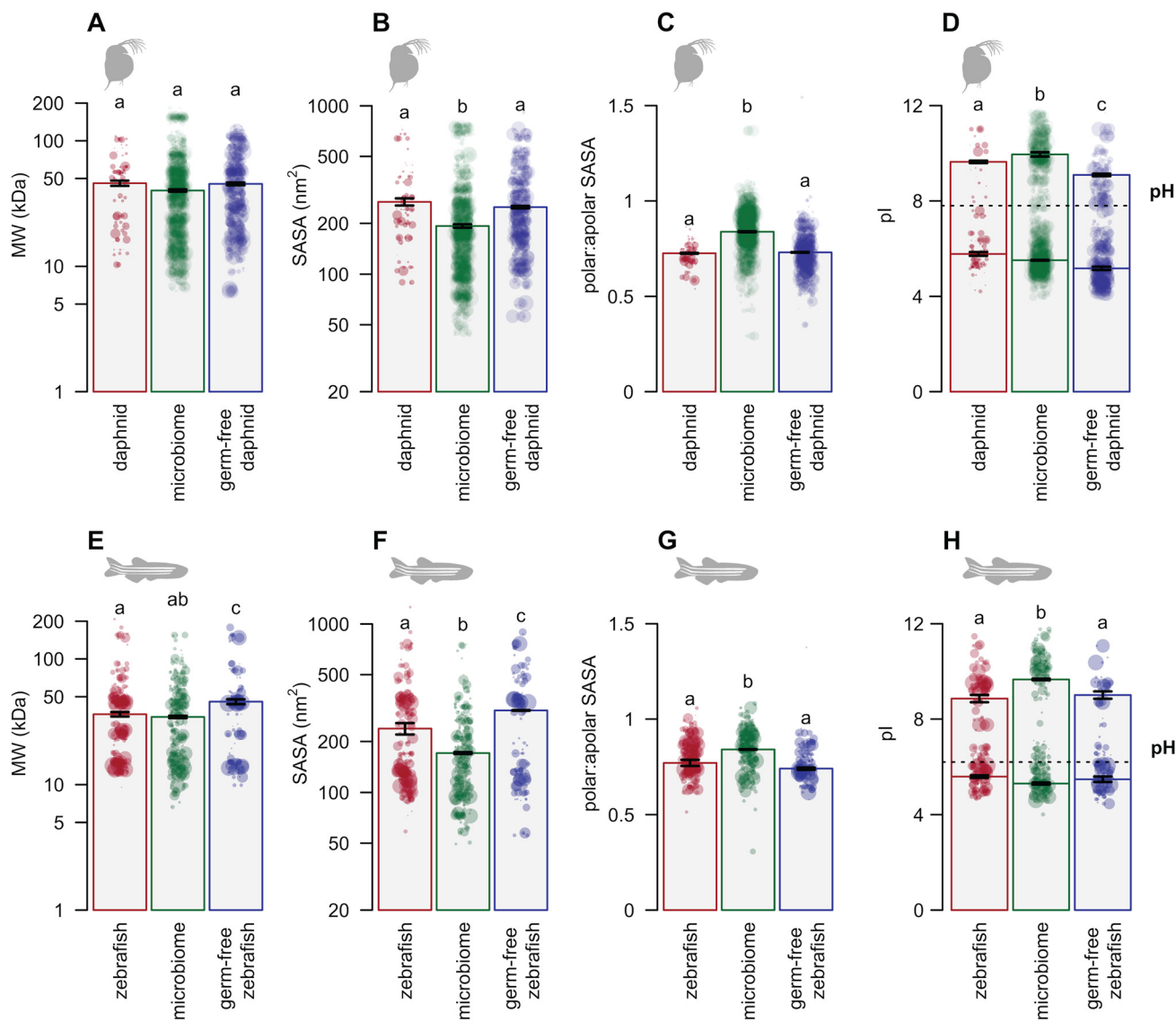


Fig. 4 Physicochemical properties of host and microbiome proteins detected in nTiO₂ eco-coronas of *D. magna* (A–D) and *D. rerio* (E–H). Subpanels present the molecular weight (A and E), solvent-accessible surface area (B and F), polar : apolar solvent-accessible surface area (C and G) and isoelectric point (D and H) of proteins. Bars represent intensity-weighted averages ($n = 3$) of proteins from microbially colonized hosts (red), microbiome proteins (green) and proteins from germ-free hosts (blue). Error bars depict the SEM. Each dot represents one protein, where the size of points scales proportionally to their log-transformed MS intensity. Bars that do not share a letter present significantly different intensity-weighted averages ($p < 0.05$). The dotted line in (D) and (H) indicate the pH of the medium. Abbreviations: MW, molecular weight; SASA, solvent-accessible surface area; pl, isoelectric point.

of proteins, as a measure of polarity, and (4) the isoelectric point (pI), to infer protein net charge. All properties were compared based on their MS intensity weighted averages.

Several physical-chemical properties differed between coronal proteins (Fig. 4) and proteins in surrounding medium (Fig. S4). For instance, coronal proteins of *D. magna* had a higher MW (43.7 ± 1.2 kDa) than proteins in the medium (37.0 ± 1.2 kDa; $F_{1,12} = 58.5$, $p < 0.001$; Fig. S4A). Under germ-free conditions, coronal daphnid proteins moreover had a larger SASA (250 ± 4.1 nm²) than proteins in the surrounding medium (226 ± 7.4 nm²; $p < 0.02$; Fig. S4B), while under colonized conditions, the pI of anionic coronal daphnid proteins was higher (5.8 ± 0.08) than the pI of

anionic proteins from the medium (5.3 ± 0.004 ; $p < 0.001$). For both *D. magna* and *D. rerio*, coronal proteins from germ-free conditions had a higher polar-to-apolar SASA ratio (0.74 ± 0.004) than proteins from the medium (0.70 ± 0.02 ; $p = 0.006$). These differences indicate that the formation of eco-coronas on nTiO₂ is a selective process.

Once adsorbed, marked differences between the physicochemical properties of host and microbiome proteins could be observed. These differences could affect the interactions between nanomaterials and their surroundings in three different ways. Firstly, coronal microbiome proteins had a smaller SASA (193 ± 4.6 nm² for *D. magna* and 171 ± 2.1 nm² for *D. rerio*) than coronal host proteins (268 ± 13



nm^2 for *D. magna* and $239 \pm 19 \text{ nm}^2$ for *D. rerio*; $p < 0.001$). A similar trend was observed for the MW of coronal microbiome and host proteins, where the MW of microbiome proteins was marginally smaller ($40.1 \pm 0.8 \text{ kDa}$ for *D. magna* and $34.5 \pm 0.8 \text{ kDa}$ for *D. rerio*) than the MW of host proteins ($45.8 \pm 2.2 \text{ kDa}$ for *D. magna* and $36.2 \pm 1.5 \text{ kDa}$ for *D. rerio*, $p = 0.07$). Likely, the smaller size and surface area of microbiome proteins allowed them to diffuse through smaller spaces that are available in between other eco-corona biomolecules, increasing the overall biomolecular density in eco-coronas. This may explain why microbiome proteins become enriched in eco-coronas relative to their surrounding medium (section 3.1).

Secondly, microbiome proteins provide an overall higher polar SASA than host proteins in eco-coronas, given the higher ratio between the polar and the apolar SASA of microbiome proteins (0.84 ± 0.002 and 0.84 ± 0.002 for *D. magna* and *D. rerio*, respectively) as compared to host proteins (0.73 ± 0.002 and 0.77 ± 0.02 , respectively; $p < 0.001$). These results suggest that microbiome proteins can increase the heterogeneity of protein coronas by providing local areas with increased polarity. Luo *et al.*⁶⁵ have mathematically demonstrated that nonlocality of polarization clouds weakens van der Waals forces acting between spherical nanoparticles. Therefore, the increased heterogeneity in polarity due to the inclusion of microbiome proteins in eco-coronas may further weaken van der Waals interaction between nanoparticles, thereby increasing the stability of nanoparticle dispersions. Assessing the environmental relevance of this finding requires follow-up research, quantifying this potential stabilizing effect experimentally. Due to the non-spherical shape and low stability of nTiO_2 , other techniques than DLS should be employed to do so. Suitable options include asymmetrical flow field-flow fractionation, two-dimensional X-ray absorption and cryogenic scanning transmission electron microscopy, as demonstrated by Monikh *et al.*⁶⁶ and Catalano *et al.*⁶⁷

Thirdly, differences between the pI of eco-corona proteins (Fig. 4D and F) indicate that most eco-corona proteins have either a net positive charge (cations, $\text{pI} > \text{pH}$) or a net negative charge (anions, $\text{pI} < \text{pH}$), even following pH fluctuations of several pH units. Such charged proteins in eco-coronas may stabilize nanomaterials *via* steric repulsion between similar charges. Based on total MS intensities, the fraction of cations in eco-coronas of *D. magna* was higher for microbiome proteins ($31.9 \pm 0.5\%$) than for host proteins ($24.5 \pm 2.4\%$; $p = 0.04$). This suggests that microbiome proteins add more cationic regions to nTiO_2 eco-coronas than host proteins. Burnand *et al.*⁶⁸ demonstrated experimentally that interactions between positively charged amino residues of eco-corona proteins and negatively charged cell membranes can facilitate the uptake of nanoparticles by cells. In view of this, the greater cationic regions provided by microbiome proteins in eco-coronas may enhance the coulombic interactions between

nanomaterials and cells, leading to higher nanomaterial uptake.

3.5 Binding partners of host and microbiome eco-corona proteins

In the final part of our study, we complement the analysis of physical and chemical properties of proteins from a functional point of view. We used Gene Ontology (GO) molecular function annotations to infer the binding partners of proteins in eco-coronas. In this ontology, binding is defined as ‘the selective, non-covalent, often stoichiometric, interaction of a molecule with one or more specific sites on another molecule’.⁶⁹ We differentiate five binding partners: cations, anions, proteins, carbohydrates and lipids.

Based on the GO analysis, we identified 163 binding proteins from *D. magna*, 610 binding proteins from the *D. magna* microbiome, 665 binding proteins from *D. rerio*, and 202 binding proteins from the *D. rerio* microbiome. The contribution of host and microbiome proteins to the total MS binding intensity in media and on TiO_2 followed the same trend as the total MS intensity of microbiome and host proteins in these samples (Fig. 2). This means that for *D. magna*, microbiome proteins had more binding partners ($41.4 \pm 2.2\%$) than host proteins ($0.7 \pm 0.06\%$; $p < 0.001$; Fig. 5A), while for *D. rerio*, host proteins had more binding partners ($15.4 \pm 4.6\%$) than microbiome proteins ($7.3 \pm 2.3\%$; $p < 0.001$; Fig. 5G). This remarkable resemblance between eco-corona and medium proteins suggests that most binding proteins generally do not play a major role in the adsorption of proteins to the nano-surface. Instead, mutual interactions between the binding proteins in eco-coronas and other eco-corona constituents, like carbohydrates and lipids, may stabilize multi-layered eco-coronas¹⁹ and could moreover enhance the biomolecular diversity of eco-coronas *via* the protein-induced recruitment of other metabolites.¹⁰

The relative contribution of hosts and their microbiomes to carbohydrate-binding proteins (Fig. 5E and K) and lipid-binding proteins (Fig. 5F and L) was remarkably different from that of cation-binding proteins (Fig. 5B and H), anion-binding proteins (Fig. 5C and I) and protein-binding proteins (Fig. 5D and J). Microbiome proteins contributed less carbohydrate and lipid-binding targets than host proteins in both media (Fig. S5) and eco-coronas (Fig. 5). Zebrafish larvae secreted particularly high concentrations of lectins ($7.05 \pm 2.38\%$ of the total MS intensity; Fig. S5K). Most of these zebrafish lectins, which also became part of eco-coronas (Fig. 5K), were galactose- and rhamnose-binding proteins. Lectins that were secreted by daphnid neonates ($0.41 \pm 0.03\%$ and $1.67 \pm 0.29\%$ of the total MS intensity under colonized and germ-free conditions, respectively; Fig. S5E) mainly included C-type lectin domain-containing proteins.

To our surprise, germ-free conditions resulted in much higher concentrations of lipid-binding proteins in *D. magna* coronas than in microbially colonized conditions (Fig. 5F). Most of these lipid-binding proteins were epididymal



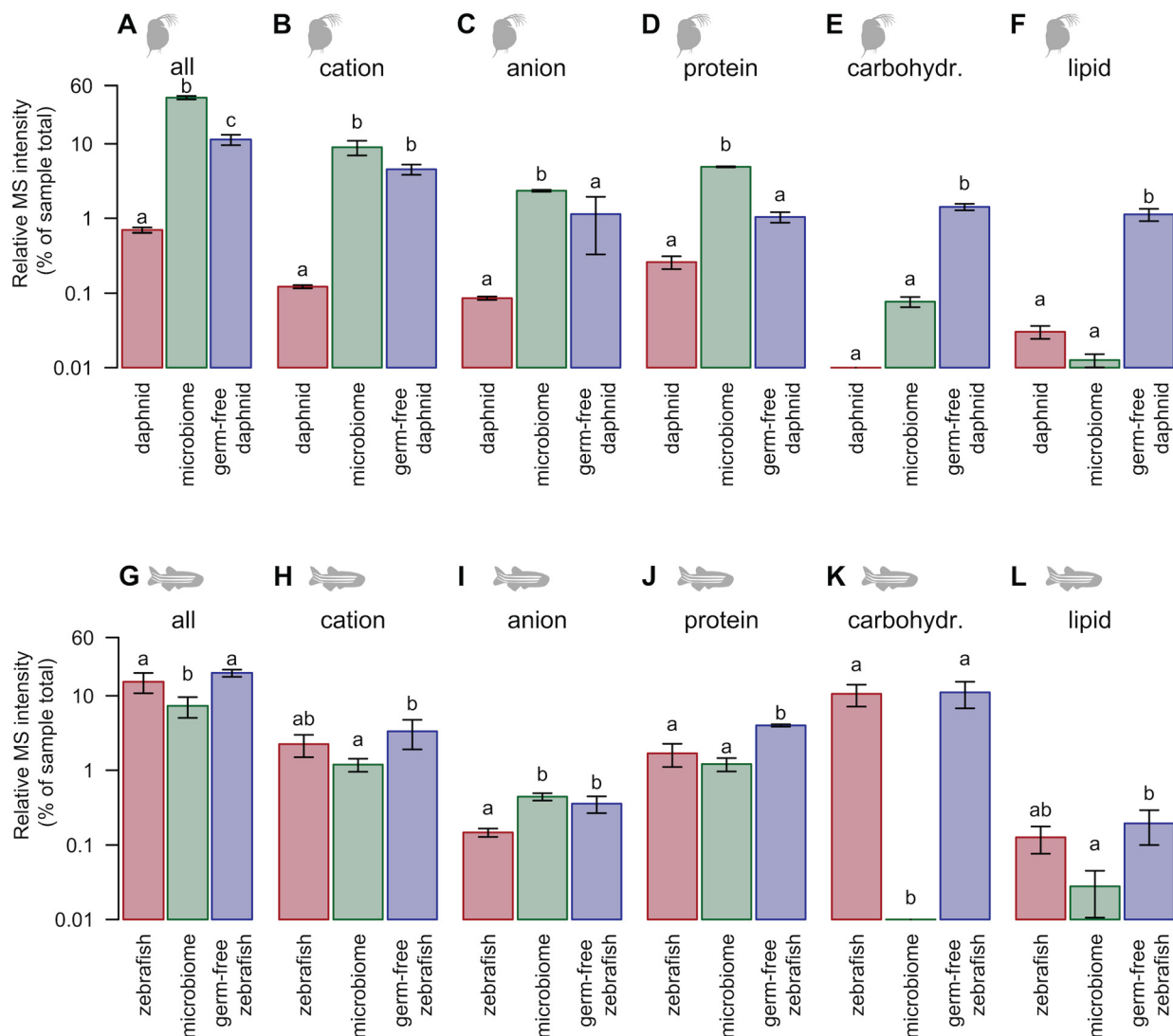


Fig. 5 Binding partners of proteins in the nTiO₂ eco-corona formed by *D. magna* (A–F) or *D. rerio* (G–L). Bars depict the total MS intensity of all proteins from microbially colonized hosts (red), their microbiome (green), or germ-free hosts (blue). Error bars depict the SEM ($n = 3$). Subpanels present proteins that have been reported or predicted to bind to biomolecules in general (A and G), or more specifically to cations (B and H), anions (C and I), proteins (D and J), carbohydrates (E and K) or lipids (F and L). Bars that do not share a letter are significantly different ($p < 0.05$). Abbreviations: carbohydr., carbohydrate.

secretory protein E1, also named Niemann–Pick intracellular cholesterol transporter 2 (NPC2). This protein functions in the transport of cholesterol and lipids from lysosomes to cells.⁷⁰ In mice, malfunction of microbiomes has been found to affect cholesterol homeostasis, resulting in higher levels of circulating cholesterol and lipids.⁷¹ Possibly, germ-free *D. magna* secreted higher concentrations of lipids, which, once adsorbed on nanomaterials, could have facilitated the additional recruitment of lipid-binding proteins. In fact, Tang *et al.*⁷² showed that cholesterol modulates coronal protein recruitment on nanoparticles by promoting the binding of apolipoproteins whilst reducing the binding complement proteins. Moreover, lipid–protein interactions have successfully been employed for the recruitment of disease-specific protein markers from blood plasma through the adsorption on lipid nanoparticles.^{73,74} Similarly, our results

indicate that lipids and lipid-binding proteins in eco-coronas could serve as markers for microbiome-dependent or nanomaterial-induced compromises to host health.

4. Conclusion

Through a combination of proteomics and metagenomic sequencing, this work demonstrates that microbiome proteins are abundant constituents of eco-coronas formed by the common ecotoxicological test species *D. magna* and *D. rerio*. The enrichment of microbiome proteins in eco-coronas of *D. magna* suggests that binding of these proteins is not a stochastic but a rather selective process. Differences in the physical and chemical properties of host and microbiome proteins, such as the smaller size of microbiome proteins, may drive this preferential inclusion of microbiome over host



proteins in eco-coronas. Once adsorbed on nanomaterials, microbiome proteins can increase the heterogeneity of eco-coronas, providing local areas with higher polarity and more cationic charge, which may shape the interactions of nanomaterials with their biotic and abiotic environment. Host and microbiome proteins can moreover bind to partners including cations, anions, carbohydrates and lipids in eco-coronas. This, in turn, may lead to the recruitment of various other types of biomolecules, which so far have received less scientific attention. Most notably, the higher abundance of lipid-binding proteins in eco-coronas of germ-free as compared to microbially colonized daphnids encourages further profiling of eco-corona lipids in relation to host microbiome integrity. Finally, the absence of microbiome proteins from intricate symbionts like *Limnohabitans* sp. suggests that proteins of such microbial taxa only become part of eco-coronas following nanomaterial internalization. Follow-up studies that do not only focus on secreted microbiome proteins in eco-coronas but also study microbiome proteins in the presence of a host therefore merit further investigation. From multiple points of view, the results of this study predict that the characterization of microbiome proteins in eco-coronas will deepen our understanding of nanomaterial exposure routes and bio-nano interactions.

Author contributions

Bregje W. Brinkmann: conceptualization, formal analysis, investigation, methodology, writing – original draft, review & editing, visualization. Zhiling Guo: conceptualization, funding acquisition, writing – review & editing. Martina G. Vijver: conceptualization, funding acquisition, writing – review & editing. Willie J. G. M. Peijnenburg: conceptualization, resources, writing – review & editing, funding acquisition. Andrew J. Chetwynd: conceptualization, investigation, methodology, writing – original draft, review & editing.

Conflicts of interest

There are no conflicts of interest to declare.

Data availability

The metagenomic sequencing data are deposited in the NCBI Sequence Read Archive under BioProject ID: PRJNA1336773 (<http://www.ncbi.nlm.nih.gov/bioproject/1336773>). Genus-level taxonomic identifications and proteomic datasets are available on Zenodo (<http://doi.org/10.5281/zenodo.1722884>).

Two supplementary information files are available. File S1 presents supplementary methods, figures and tables. File S2 presents methods and results of the experiments that were performed with CNTs. See DOI: <https://doi.org/10.1039/d5en00493d>.

Acknowledgements

The authors thank Gerda Lamers for acquiring transmission electron microscopy micrographs of the nanomaterials, Hannah Ging for protein quantification of MS samples, and Stefan Romeijn for providing technical support and equipment for the lyophilization of protein samples. This work was supported by the project ‘EcoWizard’ (ERC-C 101002123) awarded to professor Martina Vijver. The collaboration between the University of Birmingham and Leiden University was supported by a UoB-Leiden SEED fund awarded to Zhiling Guo and Willie Peijnenburg.

References

- 1 L. Wu, Y. Zhang, C. Zhang, X. Cui, S. Zhai, C. Li, H. Zhu, G. Qu, G. Jiang and B. Yan, Tuning cell autophagy by diversifying carbon nanotube surface chemistry, *ACS Nano*, 2014, **8**, 2087–2099, DOI: [10.1021/nn500376w](https://doi.org/10.1021/nn500376w).
- 2 M. Le Goas, F. Testard, O. Taché, N. Debou, B. Cambien, G. Carrot and J.-P. Renault, How do surface properties of nanoparticles influence their diffusion in the extracellular matrix? A model study in matrigel using polymer-grafted nanoparticles, *Langmuir*, 2020, **36**, 10460–10470, DOI: [10.1021/acs.langmuir.0c01624](https://doi.org/10.1021/acs.langmuir.0c01624).
- 3 A. Gallud, M. Delaval, P. Kinaret, V. S. Marwah, V. Fortino, J. Ytterberg, R. Zubarev, T. Skoog, J. Kere, M. Correia, K. Loeschner, Z. Al-Ahmady, K. Kostarelos, J. Ruiz, D. Astruc, M. Monopoli, R. Handy, S. Moya, K. Savolainen, H. Alenius, D. Greco and B. Fadeel, Multiparametric profiling of engineered nanomaterials: Unmasking the surface coating effect, *Adv. Sci.*, 2020, **7**, 1–18, DOI: [10.1002/advs.202002221](https://doi.org/10.1002/advs.202002221).
- 4 P. A. S. Kinaret, J. Ndika, M. Ilves, H. Wolff, G. Vales, H. Norppa, K. Savolainen, T. Skoog, J. Kere, S. Moya, R. D. Handy, P. Karisola, B. Fadeel, D. Greco and H. Alenius, Toxicogenomic profiling of 28 nanomaterials in mouse airways, *Adv. Sci.*, 2021, **8**, 1–15, DOI: [10.1002/advs.202004588](https://doi.org/10.1002/advs.202004588).
- 5 G. Gupta, J. Kaur, K. Bhattacharya, B. J. Chambers, A. Gazzi, G. Furesi, M. Rauner, C. Fuoco, M. Orecchioni, L. G. Delogu, L. Haag, J. E. Stehr, A. Thomen, R. Bordes, P. Malmberg, G. A. Seisenbaeva, V. G. Kessler, M. Persson and B. Fadeel, Exploiting mass spectrometry to unlock the mechanism of nanoparticle-induced inflammasome activation, *ACS Nano*, 2023, **17**, 17451–17467, DOI: [10.1021/acsnano.3c05600](https://doi.org/10.1021/acsnano.3c05600).
- 6 S. V. Kaymaz, H. M. Nobar, H. Sarigül, C. Soylukan, L. Akyüz and M. Yüce, Nanomaterial surface modification toolkit: Principles, components, recipes, and applications, *Adv. Colloid Interface Sci.*, 2023, **322**, 1–32, DOI: [10.1016/j.cis.2023.103035](https://doi.org/10.1016/j.cis.2023.103035).
- 7 K. A. Dawson and Y. Yan, Current understanding of biological identity at the nanoscale and future prospects, *Nat. Nanotechnol.*, 2021, **16**, 229–242, DOI: [10.1038/s41565-021-00860-0](https://doi.org/10.1038/s41565-021-00860-0).
- 8 I. Lynch, K. A. Dawson, J. R. Lead and E. Valsami-Jones, in *Frontiers of Nanoscience*, ed. J. R. Lead and E. Valsami-Jones, Elsevier, Amsterdam, 2014, ch. 4, vol. 7, pp. 127–156, DOI: [10.1016/B978-0-08-099408-6.00004-9](https://doi.org/10.1016/B978-0-08-099408-6.00004-9).



- 32 OECD, *Test No. 202 Daphnia sp. Acute Immobilisation Test, OECD Guidelines for the Testing of Chemicals*, OECD Publishing, Paris, 2004, DOI: [10.1787/9789264069947-en](https://doi.org/10.1787/9789264069947-en).
- 33 OECD, *Test No. 236 Fish Embryo Acute Toxicity (FET) Test, OECD Guidelines for the Testing of Chemicals*, OECD Publishing, Paris, 2013, DOI: [10.1787/9789264203709-en](https://doi.org/10.1787/9789264203709-en).
- 34 B.-Y. Lee, B.-S. Choi, M.-S. Kim, J. C. Park, C. B. Jeong, J. Han and J. S. Lee, The genome of the freshwater water flea *Daphnia magna*: A potential use for freshwater molecular ecotoxicology, *Aquat. Toxicol.*, 2019, **210**, 69–84, DOI: [10.1016/j.aquatox.2019.02.009](https://doi.org/10.1016/j.aquatox.2019.02.009).
- 35 K. Howe, M. D. Clark, C. F. Torroja, J. Torrance, C. Berthelost, M. Muffato, J. E. Collins, S. Humphray, K. McLaren and L. Matthews, *et al.*, The zebrafish reference genome sequence and its relationship to the human genome, *Nature*, 2013, **496**, 498–503, DOI: [10.1038/nature12111](https://doi.org/10.1038/nature12111).
- 36 B. Bauer, A. Mally and D. Liedtke, Zebrafish embryos and larvae as alternative animal models for toxicity testing, *Int. J. Mol. Sci.*, 2021, **22**, 1–23, DOI: [10.3390/ijms222413417](https://doi.org/10.3390/ijms222413417).
- 37 K. Toyota, C. Hiruta, Y. Ogino, S. Miyagawa, T. Okamura, Y. Onishi, N. Tatarazako and T. Iguchi, Comparative developmental staging of female and male water fleas *Daphnia pulex* and *Daphnia magna* during embryogenesis, *Zool. Sci.*, 2016, **33**, 31–37, DOI: [10.2108/zs150116](https://doi.org/10.2108/zs150116).
- 38 M. Callens, E. Macke, K. Muylaert, P. Bossier, B. Lievens, M. Waud and E. Decaestecker, Food availability affects the strength of mutualistic host–microbiota interactions in *Daphnia magna*, *ISME J.*, 2016, **10**, 911–920, DOI: [10.1038/ismej.2015.166](https://doi.org/10.1038/ismej.2015.166).
- 39 B. W. Brinkmann, B. E. V. Koch, H. P. Spaink, W. J. G. M. Peijnenburg and M. G. Vijver, Colonizing microbiota protect zebrafish larvae against silver nanoparticle toxicity, *Nanotoxicology*, 2020, **14**, 725–739, DOI: [10.1080/17435390.2020.1755469](https://doi.org/10.1080/17435390.2020.1755469).
- 40 M. van Pomeran, W. J. G. M. Peijnenburg, N. R. Brun and M. G. Vijver, A novel experimental and modelling strategy for nanoparticle toxicity testing enabling the use of small quantities, *Int. J. Environ. Res. Public Health*, 2017, **14**, 1–14, DOI: [10.3390/ijerph14111348](https://doi.org/10.3390/ijerph14111348).
- 41 K. Rasmussen, J. Mast, P.-J. De Temmerman, E. Verleysen, N. Waegeneers, F. Van Steen, J. C. Pizzolon, L. De Temmerman, E. Van Doren, K. A. Jensen, R. Birkedal, M. Levin, S. H. Nielsen, I. K. Koponen, P. A. Clausen, V. Kofoed-Sørensen, Y. Kembouche, N. Thieriet, O. Spalla, C. Giuot, D. Rousset, O. Witschger, S. Bau, B. Bianchi, C. Motzkus, B. Shivachev, L. Dimowa, R. Nikolova, D. Nihtianova, M. Tarassov, O. Petrov, S. Bakardjieva, D. Gilliland, F. Pianella, G. Ceccone, V. Spampinato, G. Cotogno, P. Gibson, C. Gaillard and A. Mech, *Titanium dioxide, NM-100, NM-101, NM-102, NM-103, NM-104, NM-105: Characterisation and physico-chemical properties*, Report No.: JRC 86291, JRC Science and Policy Reports, ISPRA, 2014, DOI: [10.2788/79554](https://doi.org/10.2788/79554).
- 42 S. Allard, M. Pinault and M. Mayne-L'Hermite, *Report on carbon nanotube samples prepared and characterized at CEA-Saclay*, DSM-IRAMIS-NIMBE-Laboratoire Edifices Nanométriques, Paris, 2015.
- 43 K. A. Jensen, Y. Kembouche, K. Loeschner and M. Correia, *SOP for probe-sonicator calibration of delivered acoustic power and de-agglomeration efficiency for in vitro an in vivo toxicological testing, Version 1.1*, Dutch National Institute for Public Health and the Environment (RIVM), Bilthoven, 2018.
- 44 K. A. Jensen, *SOP for intra- and interlaboratory reproducible measurement of hydrodynamic size-distribution and dispersion stability of manufactured nanomaterials using Dynamic Light Scattering (DLS), Version 1.1*, Dutch National Institute for Public Health and the Environment (RIVM), Bilthoven, 2018.
- 45 K. Faserl, A. J. Chetwynd, I. Lynch, J. A. Thorn and H. H. Lindner, Corona isolation method matters: Capillary electrophoresis mass spectrometry based comparison of protein corona compositions following on-particle versus in-solution or in-gel digestion, *Nanomaterials*, 2019, **9**, 1–21, DOI: [10.3390/nano9060898](https://doi.org/10.3390/nano9060898).
- 46 J. Lu, N. Rincon, D. E. Wood, F. P. Breitwieser, C. Pockrandt, B. Langmead, S. L. Salzberg and M. Steinegger, Metagenome analysis using the Kraken software suite, *Nat. Protoc.*, 2022, **17**, 2815–2839, DOI: [10.1038/s41596-022-00738-y](https://doi.org/10.1038/s41596-022-00738-y).
- 47 B. Langmead and S. L. Salzberg, Fast gapped-read alignment with Bowtie 2, *Nat. Methods*, 2012, **9**, 357–359, DOI: [10.1038/NMETH.1923](https://doi.org/10.1038/NMETH.1923).
- 48 D. E. Wood, J. Lu and B. Langmead, Improved metagenomic analysis with Kraken 2, *Genome Biol.*, 2019, **20**, 1–13, DOI: [10.1186/s13059-019-1891-0](https://doi.org/10.1186/s13059-019-1891-0).
- 49 N. A. O'Leary, M. W. Wright, J. R. Brister, S. Ciufu, D. Haddad, R. McVeigh, B. Rajput, B. Robbertse, B. Smith-White, D. Ako-Adjei, A. Astashyn, A. Badretdin, Y. Bao, O. Blinkova, V. Brover, V. Chetvernin, J. Choi, E. Cox, O. Ermolaeva, C. M. Farrell, T. Goldfarb, T. Gupta, D. Haft, E. Hatcher, W. Hlavina, V. S. Joardar, V. K. Kodali, W. Li, D. Maglott, P. Masterson, K. M. McGarvey, M. R. Murphy, K. O'Neill, S. Pujar, S. H. Rangwala, D. Rausch, L. D. Riddick, C. Schoch, A. Shkeda, S. S. Storz, H. Sun, F. Thibaud-Nissen, I. Tolstoy, R. E. Tully, A. R. Vatsan, C. Wallin, D. Webb, W. Wu, M. J. Landrum, A. Kimchi, T. Tatusova, M. DiCuccio, P. Kitts, T. D. Murphy and K. D. Pruitt, Improved metagenomic analysis with Kraken 2, *Nucleic Acids Res.*, 2016, **44**, D733–D745, DOI: [10.1093/nar/gkv1189](https://doi.org/10.1093/nar/gkv1189).
- 50 J. Lu, F. P. Breitwieser, P. Thielen and S. L. Salzberg, Bracken: estimating species abundance in metagenomics data, *PeerJ Comput. Sci.*, 2017, **3**, 1–17, DOI: [10.7717/peerj-cs.104](https://doi.org/10.7717/peerj-cs.104).
- 51 P. Breitwieser and S. L. Salzberg, Pavian: interactive analysis of metagenomics data for microbiome studies and pathogen identification, *Bioinformatics*, 2020, **36**, 1303–1304, DOI: [10.1093/bioinformatics/btz715](https://doi.org/10.1093/bioinformatics/btz715).
- 52 E. Dubois, A. N. Galindo, L. Dayon and O. Cominetti, Assessing normalization methods in mass spectrometry-based proteome profiling of clinical samples, *BioSystems*, 2022, **215–216**, 1–11, DOI: [10.1016/j.biosystems.2022.104661](https://doi.org/10.1016/j.biosystems.2022.104661).
- 53 C. Lazar, L. Gatto, M. Ferro, C. Bruley and T. Burger, Accounting for the multiple natures of missing values in



- label-free quantitative proteomics data sets to compare imputation strategies, *J. Proteome Res.*, 2016, **15**, 116–1125, DOI: [10.1021/acs.jproteome.5b00981](https://doi.org/10.1021/acs.jproteome.5b00981).
- 54 B. Bjellqvist, B. Basse, E. Olsen and J. E. Celis, Reference points for comparisons of two-dimensional maps of proteins from different human cell types defined in a pH scale where isoelectric points correlate with polypeptide compositions, *Electrophoresis*, 1994, **15**, 529–539, DOI: [10.1002/elps.1150150171](https://doi.org/10.1002/elps.1150150171).
- 55 B. Bjellqvist, G. J. Hughes, C. Pasquali, N. Paquet, F. Ravier, J. C. Sanchez, S. Frutiger and D. F. Hochstrasser, The focusing positions of polypeptides in immobilized pH gradients can be predicted from their amino acid sequences, *Electrophoresis*, 1993, **14**, 1023–1031, DOI: [10.1002/elps.11501401163](https://doi.org/10.1002/elps.11501401163).
- 56 E. Gasteiger, C. Hoogland, A. Gattiker, S. Duvaud, M. R. Wilkins, R. D. Appel and A. Bairoch, Protein Identification and Analysis Tools in the ExpPASy Server, in *The Proteomics Protocols Handbook*, ed. J. M. Walker, Humana Press, Totowa, 1st edn, 2005, pp. 571–607, DOI: [10.1385/1-59259-890-0:571](https://doi.org/10.1385/1-59259-890-0:571).
- 57 B. W. Brinkmann, W. F. Beijk, R. C. Vlieg, S. J. T. Van Noort, J. L. Colaux, S. Lucas, G. Lamers, W. J. G. M. Peijnenburg and M. G. Vijver, Adsorption of titanium dioxide nanoparticles onto zebrafish eggs affects colonizing microbiota, *Aquat. Toxicol.*, 2021, **232**, 1–13, DOI: [10.1016/j.aquatox.2021.105744](https://doi.org/10.1016/j.aquatox.2021.105744).
- 58 G. Da Silva Pescador, D. Baia Amaral, J. M. Varberg, Y. Zhang, Y. Hao, L. Florens and A. A. Bazzini, Protein profiling of zebrafish embryos unmasks regulatory layers during early embryogenesis, *Cell Rep.*, 2024, **43**, 1–24, DOI: [10.1016/j.celrep.2024.114769](https://doi.org/10.1016/j.celrep.2024.114769).
- 59 J. Ouwehand, B. W. Brinkmann, W. J. G. M. Peijnenburg and M. G. Vijver, Microbial custody: key microbiome inhabitant *Sphingomonas* alleviates silver nanoparticle toxicity in *Daphnia magna*, *FEMS Microbiol. Ecol.*, 2025, **101**, 1–8, DOI: [10.1093/femsec/fiaf061](https://doi.org/10.1093/femsec/fiaf061).
- 60 D. J. Davis, E. C. Bryda, C. H. Gillespie and A. C. Ericsson, Microbial modulation of behavior and stress responses in zebrafish larvae, *Behav. Brain Res.*, 2016, **311**, 219–227, DOI: [10.1016/j.bbr.2016.05.040](https://doi.org/10.1016/j.bbr.2016.05.040).
- 61 R. O. Cooper and C. E. Cressler, Characterization of key bacterial species in the *Daphnia magna* microbiota using shotgun metagenomics, *Sci. Rep.*, 2020, **10**, 1–11, DOI: [10.1038/s41598-019-57367-x](https://doi.org/10.1038/s41598-019-57367-x).
- 62 A. Chaturvedi, X. Li, V. Dhandapani, H. Marshall, S. Kissane, M. Cuenca-Cambronero, G. Asole, F. Calvet, M. Ruiz-Romero, P. Marangio, R. Guigó, D. Rago, L. Mirbahai, N. Eastwood, J. K. Colbourne, J. Zhou, E. Mallon and L. Orsini, The hologenome of *Daphnia magna* reveals possible DNA methylation and microbiome-mediated evolution of the host genome, *Nucleic Acids Res.*, 2023, **51**, 9785–9803, DOI: [10.1093/nar/gkad685](https://doi.org/10.1093/nar/gkad685).
- 63 E. M. Eckert and J. Pernthaler, Bacterial epibionts of *Daphnia*: a potential route for the transfer of dissolved organic carbon in freshwater food webs, *ISME J.*, 2014, **8**, 1808–1819, DOI: [10.1038/ismej.2014.39](https://doi.org/10.1038/ismej.2014.39).
- 64 F. A. Monikh, L. Chupani, M. G. Vijver, M. Vancová and W. J. G. M. Peijnenburg, Analytical approaches for characterizing and quantifying engineered nanoparticles in biological matrices from an (eco)toxicological perspective: Old challenges, new methods and techniques, *Sci. Total Environ.*, 2019, **660**, 1283–1293, DOI: [10.1016/j.scitotenv.2019.01.105](https://doi.org/10.1016/j.scitotenv.2019.01.105).
- 65 Y. Luo, R. Zhao and J. B. Pendry, van der Waals interactions at the nanoscale: The effects of nonlocality, *Proc. Natl. Acad. Sci. U. S. A.*, 2015, **111**, 18422–18427, DOI: [10.1073/pnas.1420551111](https://doi.org/10.1073/pnas.1420551111).
- 66 F. A. Monikh, N. Grundschober, S. Romeijn, D. Arenas-Lago, M. G. Vijver, W. Jiskoot and W. J. G. M. Peijnenburg, Development of methods for extraction and analytical characterization of carbon-based nanomaterials (nanoplastics and carbon nanotubes) in biological and environmental matrices by asymmetrical flow field-flow fractionation, *Environ. Pollut.*, 2019, **225**, 1–9, DOI: [10.1016/j.envpol.2019.113304](https://doi.org/10.1016/j.envpol.2019.113304).
- 67 R. Catalano, D. L. Slomberg, C. Picard, N. Hucher, V. Vidal, F. Saint-Antonin, J.-C. Hubaud, J. Rose and J. Labille, In situ determination of engineered nanomaterial aggregation state in a cosmetic emulsion – toward safer-by-design products, *Environ. Sci.: Nano*, 2021, **8**, 3546–3559, DOI: [10.1039/d1en00345c](https://doi.org/10.1039/d1en00345c).
- 68 D. Burnand, A. Milosevic, S. Balog, M. Spuch-Calvar, B. Rothen-Rutishauser, J. Dengjel, C. Kinnear, T. L. Moore and A. Petri-Fink, Beyond global charge: Role of amine bulkiness and protein fingerprint on nanoparticle–cell interaction, *Small*, 2018, **46**, 1–19, DOI: [10.1002/smll.201802088](https://doi.org/10.1002/smll.201802088).
- 69 *Oxford Dictionary of Biochemistry and Molecular Biology*, ed. A. Smith, Oxford University press, Oxford, Revised edn, 2000, pp. 1–752.
- 70 R. E. Infante, M. L. Wang, A. Radhakrishnan, H. J. Kwon, M. S. Brown and J. L. Goldstein, NPC2 facilitates bidirectional transfer of cholesterol between NPC1 and lipid bilayers, a step in cholesterol egress from lysosomes, *Proc. Natl. Acad. Sci. U. S. A.*, 2008, **105**, 15287–15292, DOI: [10.1073/pnas.0807328105](https://doi.org/10.1073/pnas.0807328105).
- 71 T. Le Roy, E. Lécuyer, B. Chassaing, M. Rhimi, M. Lhomme, S. Boudebouze, F. Ichou, J. H. Barceló, T. Huby, M. Guerin, P. Giral, E. Maguin, N. Kapel, P. Gérard, K. Clément and P. Lesnik, The intestinal microbiota regulates host cholesterol homeostasis, *BMC Biol.*, 2019, **17**, 1–18, DOI: [10.1186/s12915-019-0715-8](https://doi.org/10.1186/s12915-019-0715-8).
- 72 H. Tang, Y. Zhang, T. Yang, C. Wang, Y. Zhu, L. Qiu, J. Liu, Y. Song, L. Zhou, J. Zhang, Y. K. Wong, Y. Liu, C. Xu, H. Wang and J. Wang, Cholesterol modulates the physiological response to nanoparticles by changing the composition of protein corona, *Nat. Nanotechnol.*, 2023, **18**, 1067–1077, DOI: [10.1038/s41565-023-01455-7](https://doi.org/10.1038/s41565-023-01455-7).
- 73 L. Papafilippou, A. Claxton, P. Dark, K. Kostarelos and M. Hadjidemetriou, Protein corona fingerprinting to differentiate sepsis from non-infectious systemic inflammation, *Nanoscale*, 2020, **12**, 10240–10253, DOI: [10.1039/d0nr02788j](https://doi.org/10.1039/d0nr02788j).



- 74 M. Hadjidemetriou, J. Rivers-Auty, L. Papafilippou, J. Eales, K. A. B. Kellett, N. M. Hooper, C. B. Lawrence and K. Kostarelos, Nanoparticle-enabled enrichment of longitudinal blood proteomic fingerprints in Alzheimer's disease, *ACS Nano*, 2021, **15**, 7357–7369, DOI: [10.1021/acsnano.1c00658](https://doi.org/10.1021/acsnano.1c00658).

